

# Shape-centric Modeling for Soft Robot Inchworm Locomotion

Alexander H. Chang<sup>1</sup>, Caitlin Freeman<sup>2</sup>, Arun Niddish Mahendran<sup>2</sup>, Vishesh Vikas<sup>2</sup> and Patricio A. Vela<sup>1</sup>

**Abstract**—Soft robot modeling tends to prioritize soft robot dynamics in order to recover how they might behave. Soft robot design tends to focus on how to use compliant elements with actuation to effect certain canonical movement profiles. For soft robot locomotors, these profiles should lead to locomotion. Naturally, there is a gap between the emphasis of computational modeling and the needs of locomotion design. This paper proposes to consider modeling and computation efforts directed more toward understanding soft robot-world interactions with locomotion in mind. With a SMA-actuated inchworm as the soft robot to model and control, the framework is a combination of shape identification and geometric modeling that culminates in control equations of motion. When applied to the task of gait-based locomotion, the equations operate in a low dimensional shape-based gait space. Simulated and experimentally applied gaits for an inchworm model showed qualitatively similar outcomes, while the measured net displacement per gait cycle coincided within 9%. This result advances the idea that a shape-centric approach to soft robot modeling for control and locomotion may provide predictive locomotive models.

## I. INTRODUCTION

Soft materials in robots have several material properties of interest - they can store and release energy, absorb impacts, and increase the compliance and range of possible shape profiles using minimal actuators. This versatility of soft structures is visible in locomotion of worms and caterpillars, or in manipulation of octopus arms and elephant trunks. Soft robots achieve internal actuation using pneumatic, shape memory alloy (SMA), dielectric elastomer (DEA), and motor-tendon actuators. This coupling of passive compliance and internal actuation facilitates them to achieve shapes difficult to capture using rigid articulated schemes. However, these design elements create challenges in the control of highly deformable continuum soft robots due to difficulties modeling the robot and the robot-environment interaction. Broadly, soft robots are modeled using one of the three approaches - continuum modeling, constructing reduced order lumped parameter models, or discretizing continuum shapes. Continuum approaches consider the soft material and actuator properties to construct piece-wise continuous curvature models [1], [2], cosserat rod theory [3]–[5] models or three-dimensional finite element methods (FEM) [6]–[10]. Multiple approaches including large linear deformation models, Fast-FEM algorithms, and strain-parameterization have

been applied to circumvent their high computation cost [11]. The reduced order models construct a spring-mass-damper equivalent of a soft robot [12]–[14], or model inchworm-like robots using three-link mechanisms [15], [16]. Alternatively, discretization of soft robot shapes has also been explored to construct model-free control methods [17], [18].

This paper focuses on a particular experimental elongated-body limbless soft robot. Actuators embedded in this mobile robot are configured to accomplish inchworm-like locomotive gaits. These gaits lie in the class of rectilinear gaits, which have been thoroughly explored using rigid-body articulated robots that employ either prismatic or revolute actuation mechanisms [19]–[23]. An attractive gait synthesis approach describes these articulated gait implementations as approximations of continuum body shapes [15], [24]–[26]. Gait shapes are modeled as continuous body curves to which the articulated body may then fit. For inchworm-like motion, some manner of differential friction or ideal anchoring is presumed in order to permit productive displacement.

Soft robot implementations of inchworm-like gaits attempt to exploit their compliant bodies to achieve movement. Using fewer actuators, these robots exhibit shape profiles that require rigid articulated equivalents to have many degrees of freedom. Dynamical modeling approaches for these soft robots have been predominantly FEM-based, choosing to focus on shape deformations occurring as a result of internal stresses and actuation forces applied to the body. The emphasis neglects body-environment interactions that lead to locomotion as a consequence of cyclic body shape changes. Alternative strategies, particularly targeted to elongated body mechanisms, employ cosserat rod theory [27], [28]; body-environment interactions, here, take the form of motion constraints at particular points along the elongated robot body to model locomotion. While a subset of inchworm-like robots employing static anchoring mechanisms may be modeled in this manner, body-environment frictional forcing is the more appropriate mechanism to model locomotion for many soft robot designs.

Collectively, these approaches focus on generalizability to a wide scope of deformable continuum robots. Advantages associated with specialization to particular robot anchorings, such as lower dimensional shape space representations and tractability for gait synthesis, are less emphasized. Models characterizing soft robot manipulators, however, illustrate the benefit to employing model parameterizations specialized to the underlying actuator configuration of a robot [2]. Motion of the end-effector frame is effectively captured as a function of the robot's shape parameters; these, in turn, may then be expressed with respect to the underlying robot

1: The authors are with the Institute for Robotics and Intelligent Machines (IRIM) and School of Electrical and Computer Engineering, Georgia Institute of Technology, Atlanta, GA, USA. Email: alexander.h.chang@gatech.edu, pvela@ece.gatech.edu

1: The authors are with the Department of Mechanical Engineering, University of Alabama, Tuscaloosa, AL, USA. Email: clfreeman7@crimson.ua.edu, anmahendran@crimson.ua.edu, vvikas@eng.ua.edu  
This work was supported by NSF grants #1562911, #1830432

actuation scheme. For locomotion and control, models that express locomotive outcomes as a function of the robot's prescribed shape trajectories, especially in frictional environments, would result in similarly useful group motion models. For inchworm-inspired soft robots exploiting differential friction, capturing its effects on the robot body frame will allow for meaningful prediction and control synthesis.

**Contribution.** We derive gait-based equations of motion for an elongated-body, soft robot whose 2-SMA actuator configuration permits it to accomplish inchworm-like motion. A shape-centric modeling framework [26], [29], previously applied to articulated snake-like robots, is re-purposed and specialized, here, to model the rigid motion of the body frame for this soft robot. By design, the model focuses on robot group (locomotive) dynamics, as a function of the underlying shape changes that drive it. Specialization to a particular robot's actuator scheme facilitates locomotive predictions -in frictional environments- corresponding to prescribed input actuator signals.

The shape profile of the robot is first modeled by the superposition of two time-varying body curves, whose structure is inspired by the beta probability density function (PDF). Each curve is a basis function corresponding to actuation by a particular robot SMA. Mapping the shape profile into the plane of locomotion yields quantities necessary to model the body frame dynamics of the robot. Incorporating a body-ground friction model then yields a shape-centric model of the inchworm soft robot capturing its locomotive behavior as a function of prescribed shape trajectories. The original infinite-dimensional shape space of the robot drops to a finite dimensional subspace naturally restricted to the achievable shapes associated to the robot's actuation, which is connected to the rigid body mechanics of the robot's frame. Qualitative comparison of experimentally measured trajectories to those predicted by the shape-centric model serve as validation.

## II. INCHWORM-LIKE SOFT ROBOT

### A. Morphology Design and Mechatronics

Fabrication of a multi-material, SMA-actuated inchworm soft robot with bidirectional locomotion ability poses challenges relating to morphology design (shape change and frictional manipulation) and mechatronics (integration of multi-material components) [30], [31].

*Morphology Design.* Broadly speaking, locomotion is achieved by optimizing forces at different parts of the robot body [32]. This can be achieved using multiple strategies, chiefly by manipulating frictional interactions or the shape of the robot body (thereby altering its center of mass and moment of inertia). Our robot has Differential Friction Mechanisms (DFMs) located at each end that change the frictional interaction with the locomotion surface based on the contact region. This friction manipulation is conceptually equivalent to a Coulomb friction model where the friction is initially high (static) and then becomes low after a certain amount of bending (dynamic). The DFM, Fig. 1, comprises distinct materials, one with low and the other with high friction

coefficients,  $\mu_{low}$  and  $\mu_{high}$ , respectively. The coefficient of friction of the DFM  $\mu_{DFM}$  changes with robot shape when the angle  $\psi$  between the tangent at the end and the surface exceeds the critical contact angle  $\psi^*$  dependent on design parameters  $H$  (height to center of DFM's defining circle) and  $h$  (cavity height), as illustrated in Fig. 1(a).

$$\mu_{DFM} = \begin{cases} \mu_{low} & \psi \leq \psi^* \\ \mu_{high} & \psi > \psi^* \end{cases}, \quad \psi^* = \cos^{-1} \left( \frac{H}{h} \right)$$

For a given body length, the robot's workspace (shape change) is determined by the body cavity characteristics and placement of the SMA actuators, as shown in Fig. 1. The cavity height  $h$ , width  $w$  and number  $m$  are geometrically related to each other as  $w = \frac{2h}{m} \sin^{-1} \left( \frac{\sigma_{min}}{2R} \right)$ , where  $R$  is the maximum desired bending curvature beyond which the robot experiences high stiffness. Additionally, the cavity design optimizes stiffness to enable shape change for the given actuation and body relaxation upon deactivation to allow the SMA coils to extend back their natural states. For the experimental robot,  $m = 12$  cavities of width  $w = 3.3$  mm and height  $h = 3$  mm are uniformly placed with  $H = 5$  mm. The rectangular shape of the cavities satisfies stiffness design requirements for the SMA actuators. Actuator placement is determined by (a) required airflow for actuator cooling, and (b) required overlap to ensure a smooth robot shape.

*Mechatronics.* The inchworm soft robot is fabricated by casting curable rubber silicone (Smooth-on FAST Dragon Skin™ 10) in a 3D-printed mold with removable pi-

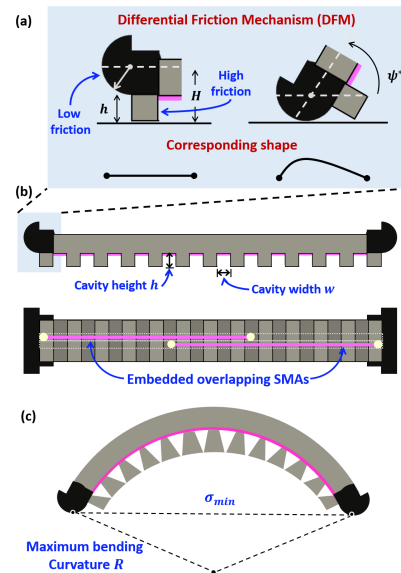


Fig. 1: Inchworm soft robot components. (a) Differential Friction Mechanisms (DFMs) located at the two ends allow the robot to change its coefficient of friction as a function of the shape. (b) Two overlapping SMA are embedded inside the soft body with cavities. (c) The cavities control bending stiffness and maximum bending curvature, and facilitate cooling of the actuators upon deactivation.

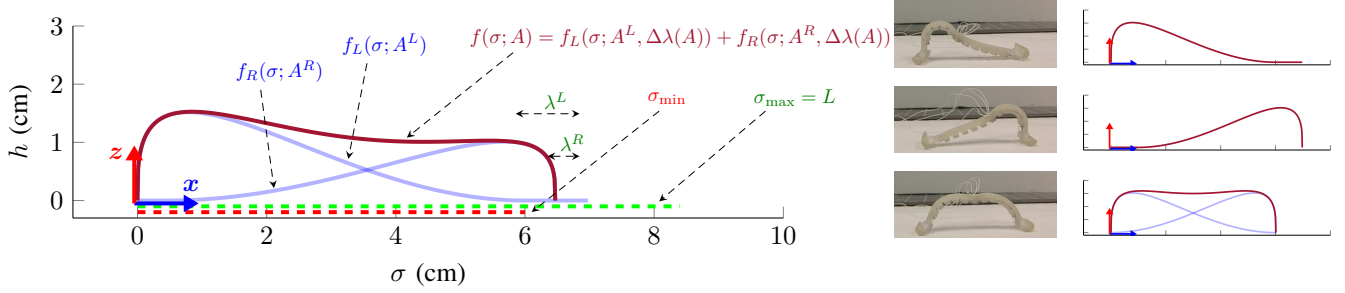


Fig. 2: **Left:** Depiction of the shape representation as a height function over the ground plane, where two basis curves  $f_L$  and  $f_R$  define the impact of left and right side actuation. All geometry is relative to the left foot reference frame, the minimum inter-feet length  $\sigma_{\min}$  (both sides maximally actuated) and the maximum inter-feet length  $\sigma_{\max}$  (both sides not actuated). Under actuation by the left side  $A^L$ , the right foot will be at  $\sigma + \lambda^L$ . Under an added actuation by the right side  $A^R$ , the right foot will come closer to  $\sigma + \lambda^L - \lambda^R$ . The right side depicts images taken of an inchworm robot with maximal left, right, and left+right actuation, plus the comparable shape in the beta distribution shape space.

$$f_L(\sigma; a, \delta) = \begin{cases} h(\sigma; a, 0), & \sigma \in [0, \sigma_{\min}] \\ 0, & \sigma \in (\sigma_{\min}, \sigma_{\min} + \delta] \end{cases} \quad \text{and} \quad f_R(\sigma; a, \delta) = \begin{cases} 0, & \sigma \in [0, \delta] \\ h(-\sigma; a, \delta), & \sigma \in (\delta, \sigma_{\min} + \delta] \end{cases}. \quad (1)$$

ano wire to create channels for the SMA actuators (BioMetal®Helix BMX 150) and ultra-flexible wires (Jag-SUPERFLEX™) that do not hinder the robot's locomotion ability. The low-friction DFM-element is printed using Eastman Amphora™ AM3300 3D polymer that is adhered at the ends of the body using mechanical locking and chemical adhesion (Smooth-on Sil-Poxy™ silicone adhesive). The actuators are controlled using a Seeeduino XIAO microcontroller and an H-Bridge with 8V power supply, and LEDs are incorporated to synchronize with the visual tracking feedback. The SMA coil actuators compress due to joule heating and effect bending of the robot body. The SMA returns to the natural extended state as it naturally cools due to heat dissipation with help of the elastic energy of the bend. Fabrication is time and cost-efficient (about 4.5 hrs) and allows for a wide range of soft (e.g. silicone or foam) and rigid materials for the DFM-element.

### III. INCHWORM GAIT

The design of the soft robot is meant to elicit a specific shape response known to result in locomotion, with the actuators explicitly controlling the shape. This section describes how the resulting shape space is modeled for the inchworm robot when placed on a flat surface. Fig. 2 contains images of an inchworm robot under actuation. For flat ground, the shape profile can be described by a height function defined over the left to right foot line on the ground plane.

With the aim of obtaining a low-dimensional shape model, we determined that a good basis function for representing the effect of actuation was the beta distribution. The equation for the beta distribution is

$$h(\sigma; a, \alpha, \beta, \sigma_{\min}) = a \cdot \frac{\left(\frac{\sigma}{\sigma_{\min}}\right)^{\alpha-1} \left(1 - \frac{\sigma}{\sigma_{\min}}\right)^{\beta-1}}{D(\alpha, \beta)}, \quad (2)$$

where the denominator is,

$$D(\alpha, \beta) = \Gamma(\alpha)\Gamma(\beta) / \Gamma(\alpha + \beta). \quad (3)$$

$\Gamma(\cdot)$  is the Gamma function,  $\sigma$  denotes distance along the abscissa defined by the left-right foot line, and  $\sigma_{\min}$  denotes the minimum length along the abscissa over which the beta function may be raised from the 'ground level'. The constants  $\alpha$ ,  $\beta$ ,  $\sigma_{\min}$ , and  $\sigma_{\max}$  are determined by material and geometric properties of the robot established by the fabrication process. The constants  $(\alpha, \beta)$  describe the shape of the basis functions, while  $\sigma_{\min}$  and  $\sigma_{\max}$  determine the support. The constant  $\sigma_{\max} = L$ , is the length of the inchworm. The constant  $\sigma_{\min}$  is the foot distance under maximum actuation by both SMAs. We define two basis functions, one for each foot, such that the actuation space  $A \in \mathbb{R}^2$  scales their amplitudes.

The presumed manufacturing process of the robot is such that SMA activation will not contract nor lengthen the robot under actuation. Rather, the bottom side cavities promote bending of the robot during activation. Under this assumption, any valid actuation profile will lead to feet separation distances in  $[\sigma_{\min}, \sigma_{\max}]$ . The fixed length of the inchworm acts as a constraint on the shape that results from actuation by  $A$ .

#### A. Recovering Shape from Actuation

The length constraints define the shape parameters  $\lambda$ , which specify the support of the robot's curve parameter  $\sigma$ . Actuation under  $A$  will result in an inter-feet length of  $\sigma_{\min} + \Delta\lambda$  where  $\Delta\lambda = \lambda^L - \lambda^R$  as depicted in Fig. 2. The shape space basis functions  $f_L$  and  $f_R$  are given in (1), and use the inchworm adapted beta distribution

$$h(\sigma; a, \delta) = a \cdot \frac{\left(\frac{(\sigma-\delta)}{\sigma_{\min}}\right)^{\alpha-1} \left(1 - \left(\frac{(\sigma-\delta)}{\sigma_{\min}}\right)\right)^{\beta-1}}{D(\alpha, \beta)},$$

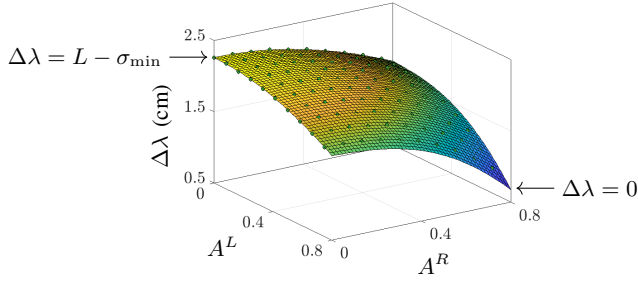


Fig. 3: Right foot offset parameter  $\Delta\lambda(A)$  using a polynomial fit. The RMSE is  $0.0054 \text{ cm}^2$ . Parameters  $\alpha = 2.0$ ,  $\beta = 2.3$ ,  $\sigma_{\min} = 6.636 \text{ cm}$ ; these values will apply to all figures and results presented.

where the  $\alpha$ ,  $\beta$ , and  $\sigma_{\min}$  terms are fixed constants. The right SMA basis function  $f_R(\sigma; A^R, \delta)$  is the beta distribution flipped left-right and shifted horizontally by  $\delta$ . The main challenge is to compute  $\lambda = (\lambda^L, \lambda^R) \in \mathbb{R}^2$  from  $A \in \mathbb{R}^2$ .

Recovery of  $\lambda$  is a two-step process starting with the left foot since it is the origin of the body frame. First, let only the left SMA be activated leading to a raised segment whose functional form is  $f_L(\sigma; \lambda^L)$ . The robot length is

$$\text{ArcLen}(f_L; A) = \int_{\sigma=0}^{\sigma_{\min}} \sqrt{1 + \left( \frac{\partial}{\partial \sigma} f_L(\sigma; A^L, 0) \right)^2} d\sigma. \quad (4)$$

Then,  $\lambda^L = \text{root}_\ell(\text{ArcLen}(f_L; A, 0) + \ell - L)$  for  $\ell \in [0, L - \sigma_{\min}]$  solves for the right foot location for the given actuation. In the absence of actuation by  $A^R$ ,  $\lambda^L$  measures how much beyond the minimum  $\sigma_{\min}$  the domain of the curve parameter should be defined to give the fixed robot length  $L$  (under the assumption that this portion has ground contact). In the case of right SMA actuation, the robot length is now

$$\text{ArcLen}(f; A, \lambda(\ell)) = \int_{\sigma=0}^{\sigma_{\min} + \Delta\lambda} \sqrt{1 + \left( \frac{\partial}{\partial \sigma} f(\sigma; A) \right)^2} d\sigma, \quad (5)$$

for a specific  $\ell$  such that  $\lambda(\ell) = (\lambda^L, \ell)$ . Activation of the right SMA reduces the domain of  $\sigma$  by  $\lambda^R = \text{root}_\ell(\text{ArcLen}(f; A, \lambda(\ell)) - L)$  for  $\ell \in [0, L - \sigma_{\min} - \lambda^L]$ . Once computed, the domain of support for the shape curve parameter  $\sigma$  is  $[0, \sigma_{\min} + \Delta\lambda] = [0, \sigma_{\min} + \lambda^L - \lambda^R]$ .

To avoid repeatedly computing these values when integrating the dynamics of a given soft robot, we pre-compute them over the domain of actuation for some fixed gridding in  $A$ , then fit the resulting output values to a thin-plate spline. Since the difference  $\Delta\lambda$  is the important variable, we regress over its value. Fig. 3 depicts the regression surface of  $\Delta\lambda$  for an inchworm model. The actual inchworm shape is:

$$f(\sigma; A) = f_L(\sigma; A^L, \Delta\lambda(A)) + f_R(\sigma; A^R, \Delta\lambda(A)). \quad (6)$$

### B. Inchworm Gaits

An inchworm gait is a cyclic path in the actuation space, which should lead to movement of the inchworm. The typical gait will start at zero actuation  $A = (0, 0)$  then maximal

actuation of one side  $A = (\bar{a}, 0)$ , maximal actuation of the second side  $A = (\bar{a}, \bar{a})$ , relaxation of the first side  $A = (0, \bar{a})$ , and conclude with relaxation of the second side  $A = (0, 0)$ . While specific waypoints were given in this description, there is freedom to choose the form, phasing, and duration of these actuation amplitudes. Reversing the cycle ordering moves the robot in the opposite direction. The structure of the cycle should respect the constraints associated with SMA thermo-mechanical properties and be slow enough to keep the robot shape movement near quasi-static equilibrium. For example, fast bang-bang actuation is not recommended since it can lead to ballistic motion. Modeling, here, will presume the shape profile (6) remains quasi-statically mechanically stable; evolution of this shape over time drives the (planar) group dynamics of the robot, derived in Section IV.

## IV. LOCOMOTIVE DYNAMICS

We model the inchworm robot as a mechanical system with symmetry, in the plane of locomotion, whose pose is captured by a shape component,  $A \in M = \mathbb{R}^2$ , and a group component,  $g \in SE(2)$ . Combined, the two components define a principal bundle.  $\xi^b = g^{-1}\dot{g}$  and  $p$  denote body velocity and momentum, respectively. The idea is to establish locomotion dynamics on the group sub-state as influenced by the shape kinematics (e.g. shape sub-state). We presume, here, that the shape is fully controlled and can be modeled based on the previous sections. The reduced Lagrange-d'Alembert dynamics for the shape + group are [33]:

$$\begin{Bmatrix} \dot{A} \\ \dot{g} \\ \dot{p} \end{Bmatrix} = \begin{Bmatrix} u \\ g \left( \Omega^b - \mathcal{A}_{loc}(A)\dot{A} \right) \\ \text{ad}_{(\Omega^b - \mathcal{A}_{loc}(A)\dot{A})}^* p + \mathcal{F}^b(A, p, \dot{A}) \end{Bmatrix}, \quad (7)$$

where  $u$  is the shape space control signal,  $\Omega^b$  is the vertical body velocity,  $p = \mathbb{I}_{lock}(A)\Omega^b$  is the vertical body momentum and  $\mathbb{I}_{lock}(\cdot)$  is the locked inertia tensor, and  $\mathcal{A}_{loc}(A)\cdot\dot{A}$  is the local principle connection.  $\mathcal{F}^b$  is the net external wrench acting on the body frame from robot-world interactions.

The connection form splits the body velocity  $\xi^b$  into horizontal and vertical components,

$$\xi^b = \Omega^b - \mathcal{A}_{loc}(A)\dot{A} = \mathbb{I}_{lock}^{-1}(A) - \mathcal{A}_{loc}(A)\dot{A}. \quad (8)$$

The horizontal component,  $-\mathcal{A}_{loc}(A)\dot{A}$ , describes the free space motion of the body due to shape changes in the locomotion plane. The vertical component  $\Omega^b$  is driven by external forcing. Lastly, the dual adjoint operation for the planar, generalized momentum  $p$  in (7) captures Coriolis effects in the system,

$$\text{ad}_{\xi^b}^* p = \begin{bmatrix} 0 & \xi_\omega^b & 0 \\ -\xi_\omega^b & 0 & 0 \\ \xi_y^b & -\xi_x^b & 0 \end{bmatrix} \begin{Bmatrix} p_x \\ p_y \\ p_\omega \end{Bmatrix}. \quad (9)$$

In the context of straight line motion, it outputs the zero vector.

These equations will be specialized, in this section, to model the locomotive dynamics of the inchworm soft robot.

Though the equations may be somewhat complex for the study at hand, we are familiar with them and can quickly derive equations of motion for systems that evolve along a line only. Future work aims to add lateral curvature into the gait shape to induce turning, whereby non-trivial Coriolis effects will then have to be considered. Starting with these equations permits extension to richer locomotion scenarios.

1) *Locked Inertia Tensor*: The locked inertia term, for the inchworm gait shape (in the  $x$ - $y$  locomotion plane) is

$$\begin{aligned} \mathbb{I}_{lock} &= \int_0^{\sigma_{\min} + \Delta\lambda} \left[ \begin{array}{c|c} \mathbb{1} & \mathbb{J}d(\sigma) \\ \hline -d^T(\sigma)\mathbb{J} & d^T(\sigma)d(\sigma) \end{array} \right] \cdot \rho(\sigma) d\sigma \\ &= \int_0^{\sigma_{\min} + \Delta\lambda} \left[ \begin{array}{c|c} \mathbb{1} & 0 \\ \hline 0 & \sigma \\ & \sigma^2 \end{array} \right] \cdot \rho(\sigma) d\sigma. \end{aligned}$$

where  $\rho(\sigma)$  is the mass density function (described next),

$$\mathbb{J} = \begin{bmatrix} 0 & -1 \\ 1 & 0 \end{bmatrix}, \text{ and } d(\sigma) = \begin{bmatrix} 0 \\ \sigma \end{bmatrix} \in E(2).$$

### A. Connection Form

Deriving the connection form for the inchworm is more complex than for the snake [23]. Here, we use a center of mass (CoM) trick for deriving it. By design, the inchworm is capable of traveling in a single direction, along the locomotion plane  $x$ -axis; we restrict our attention to its CoM projection along this axis  $\text{CoM}_x$ . In a free-space context, the CoM must remain static (w.r.t. the spatial frame) and the body frame must instead move such that the CoM (computed w.r.t. the body frame) remains static w.r.t. the spatial frame under changes in shape. In other words,

$$\mathcal{A}_{loc}(A) = -\nabla \text{CoM}_x(A). \quad (10)$$

Below, we derive  $\text{CoM}_x$  and regress its form as a surface fit, from which a numerical estimate of  $\text{CoM}_x$  follows.

1) *Density Profile*: Computing  $\text{CoM}_x$  requires the soft robot density profile. The density profile in the locomotion plane is

$$\rho(\sigma) = \rho_0 \sqrt{1 + \left( \frac{\partial}{\partial \sigma} f(\sigma; A) \right)^2}, \quad (11)$$

for  $\sigma \in [0, \sigma_{\min} + \Delta\lambda]$ . It assumes uniform material density along the length of the robot, which is roughly correct given the inchworm's symmetric and patterned structure.

2) *Center of Mass*: The center of mass projection  $\text{CoM}_x$  of the inchworm in the  $x$ -axis of the locomotion plane is computed numerically. Given the actuation state  $A \in \mathbb{R}^2$ , its associated  $\Delta\lambda$ , and the density profile along this length (11), calculation of the center of mass over a grid gives the seed values for polynomial regression. The surface fit (closely) approximates  $\text{CoM}_x$  with respect to  $A$  (see Fig. 4, left) based on values used in Fig. 3 and  $\rho_0 = 4.8$  g/cm.

The gradient of the  $\text{CoM}_x$  surface fit characterizes motion of  $\text{CoM}_x$  in the local body frame (rigidly attached to the left foot), with respect to differential changes in the actuation parameter  $A$ . This gradient vector field  $\nabla \text{CoM}_x(A)$  is plotted in Fig. 4. It simultaneously characterizes the free-space velocity of the body frame under arbitrary gait shape changes.

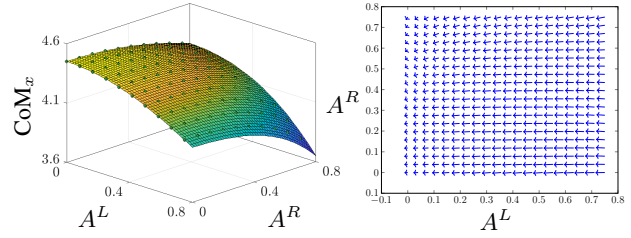


Fig. 4: **Left**: Polynomial surface fit for  $\text{CoM}_x(A)$ ; RMSE is  $0.0006 \text{ cm}^2$ . **Right**: Computed  $\text{CoM}_x$  gradient vector field.

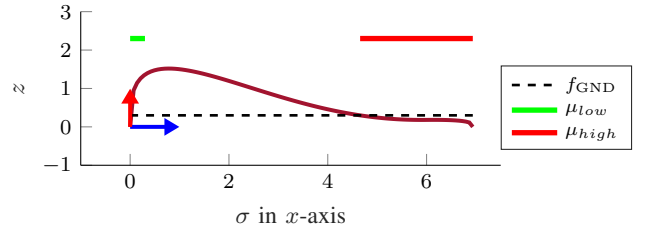


Fig. 5: Body-ground contact segments are defined by the zero crossings of  $f(\sigma; A) - f_{\text{GND}}$ .  $f(\sigma; A)$  is depicted by the brown curve. Red and green lines illustrate contact segments with friction coefficients  $\mu_{\text{high}}$  and  $\mu_{\text{low}}$ , respectively.

Because  $\text{CoM}_x$  must remain stationary (w.r.t. a spatial frame) in free-space scenarios, the body frame must instead move, hence (10).

### B. Friction Modeling

The net wrench  $\mathcal{F}^b$  acting on the body frame, in (7), is integrated from external forcing acting along the continuous gait shape (in the  $x$ - $y$  locomotion plane). External forcing, here, takes the form of frictional forces resulting from interactions between body and ground. These will then be integrated to compute  $\mathcal{F}^b$  acting at the body frame; numerical integration of (7) then yields follow-on locomotive trajectories induced by each frictional forcing model. Importantly, since the shape space trajectory  $A(t)$  is known from the gait, only the  $(g, p)$  subspace is integrated.

1) *Body-ground Contact*: Body-ground contact segments are defined to be segments of the body that have **not** been raised above the ground height threshold  $f_{\text{GND}}$ . With respect to the gait shape arc length parameter  $\sigma$ , they are

$$\mathcal{C} = \{\sigma : \sigma \in [0, \sigma_{\min} + \Delta\lambda] \wedge f(\sigma; A) \leq f_{\text{GND}}\}. \quad (12)$$

Root-finding operations compute the ground height threshold crossings (i.e. the start and end points of ground contact segments), as illustrated in Fig. 5. We additionally impose a minimum body-ground contact segment length  $\bar{c}_{\min}$ . The root finding operation may return contact segment lengths that shrink below  $\bar{c}_{\min}$ . The minimum length correction serves to guarantee that the two feet of the robot have non-trivial contact length. When corrected to the minimum, the friction profile will be associated to the low friction design. Otherwise, the high friction model is presumed to hold.

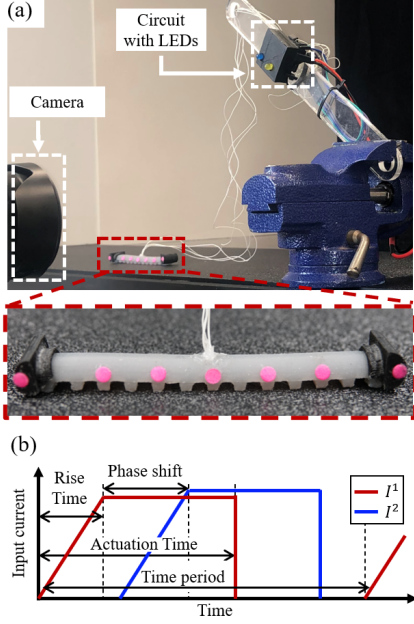


Fig. 6: (a) Experimental setup includes a tethered SMA inchworm robot with seven visual markers for tracking. LEDs are included for signal synchronization between the microcontroller and video. (b) The two SMAs are actuated with a phase shift between them using an asymmetric trapezoid control signal to satisfy the assumption of quasi-static locomotion.

2) *Viscous Friction Model*: For simplicity, we will use a viscous friction model and leave other models to a future derivation. When computing viscous frictional forces acting on each body segment in ground contact, all body positions residing within the same contact segment are characterized by the same (local) velocity, relative to the body frame,

$$v^b(\sigma) = \begin{cases} (\Delta\lambda) & \sigma \in \mathcal{C}^{\text{right}}, \text{ right contact segment} \\ 0 & \sigma \in \mathcal{C}^{\text{left}}, \text{ left contact segment} \end{cases} \quad (13)$$

Note that  $(\Delta\lambda)$  can be computed using the gradient of the regressed function much like was done with the connection form. Under linear motion, the velocities of body contact regions in the world frame are

$$v(\sigma) = \xi_x^b + v^b(\sigma) \text{ for } \sigma \in \mathcal{C}^{\{\text{left}, \text{right}\}}. \quad (14)$$

The net frictional wrench acting at the body frame is

$$\mathcal{F}_x^b = \sum_{i \in \{\text{left}, \text{right}\}} \left( \int_{\sigma \in \mathcal{C}^i} f^i(\sigma) \cdot d\sigma \right), \quad (15)$$

where frictional forcing acting at each location  $\sigma$  on a contact segment  $\mathcal{C}^i$  is

$$f^i(\sigma) = -\mu (\xi_x^b + v^b(\sigma)), \quad i \in \{\text{left}, \text{right}\}. \quad (16)$$

The friction profile to use,  $\mu_{\text{low}}$  or  $\mu_{\text{high}}$ , depends on shape. Both friction values are assumed constant over the gait; the model implicitly assumes isotropic body-ground frictional effects.

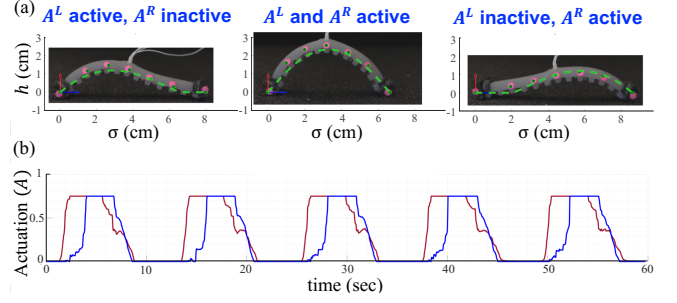


Fig. 7: (a) Calibration of the shape function uses the 3 images to measure  $(\lambda^L, \lambda^R, \sigma_{\min})$  then estimate the  $(\alpha, \beta)$  parameters of the Gamma function. Green dots depict tracked marker positions while dashed green depicts the estimated inchworm shape,  $f(\sigma; A^L, A^R)$ . (b) As the SMA inchworm moves, the actuation parameters  $A \in \mathbb{R}^2$  are estimated using least squares fit on (6). The red and blue waveforms depict the estimated signals,  $A^L(t)$  and  $A^R(t)$ , respectively.

## V. EXPERIMENT

This section describes locomotion experiments on a fabricated inchworm robot, with a periodic gait applied to the SMA actuators. It also simulates the effect of a similar gait signal applied to an inchworm modeled by the equations described in earlier sections. The model parameters from the actual inchworm are used in simulation. The gait signals and the resulting locomotion profile of the rigid body frame in the  $x$  direction are plotted for both cases. Comparison is made between the two.

### A. Actual SMA Inchworm

The experimental setup, shown in Fig. 6, consists of a camera located parallel to the locomotion plane and the soft robot with seven visual markers. Given the thermal activation of SMAs, in most natural environments, they require more time to deactivate (relax) than to activate. To ensure symmetric actuation-deactivation while satisfying the quasi-static motion assumption, SMAs are controlled using an asymmetric trapezoidal signal with a phase shift between them. For a given time period, this periodic signal implements ramp activation with step deactivation with a predetermined rise time.

For model calibration, static parameters  $\lambda^L, \lambda^R$ , and  $\sigma_{\min}$  are respectively measured from the three still images shown in Fig. 7(a) in the following order: (i)  $A^L$  fully activated,  $A^R$  inactive, (ii)  $A^L$  and  $A^R$  both fully activated, and (iii)  $A^L$  inactive,  $A^R$  fully activated. The robot body length  $\sigma_{\max} = L$  is measured using the still image of the robot where  $A^L$  and  $A^R$  are both inactive. Thereafter, the Gamma function parameters  $(\alpha, \beta)$  are obtained using a least-squares fit. For the given robot with  $\lambda^L = 79.9$  mm,  $\lambda^R = 86.1$  mm,  $\sigma_{\min} = 66.3$  mm,  $L = 89$  mm, the calibration results in  $\alpha = 2, \beta = 2.3$ . The time-varying actuation parameters  $A \in \mathbb{R}^2$  are then estimated using a least-squares fit of the visual markers for each frame, illustrated in Fig. 7(b). Please see also the accompanying video.

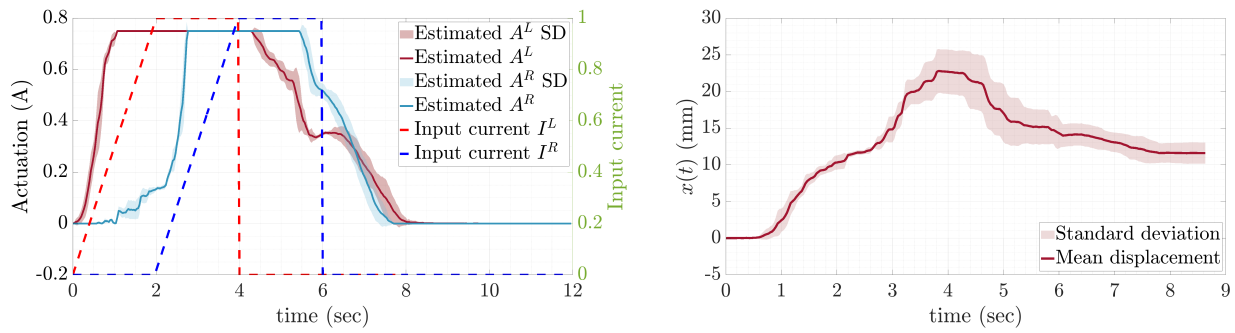


Fig. 8: **Left:** The estimated actuation  $A$  (left  $y$ -axis) follows an almost symmetric trapezoidal pattern. Experimentally, the discrepancy between the rise and fall results from non-linearities in the joule heating and natural cooling of the SMAs. The input current (right  $y$ -axis) is normalized for the microcontroller PWM value. **Right:** The trapezoidal activation results in positive displacement of the left foot frame until the left SMA current is shut off. Thereafter, the frame regresses. It experiences approx. 13.2% body length displacement per gait.

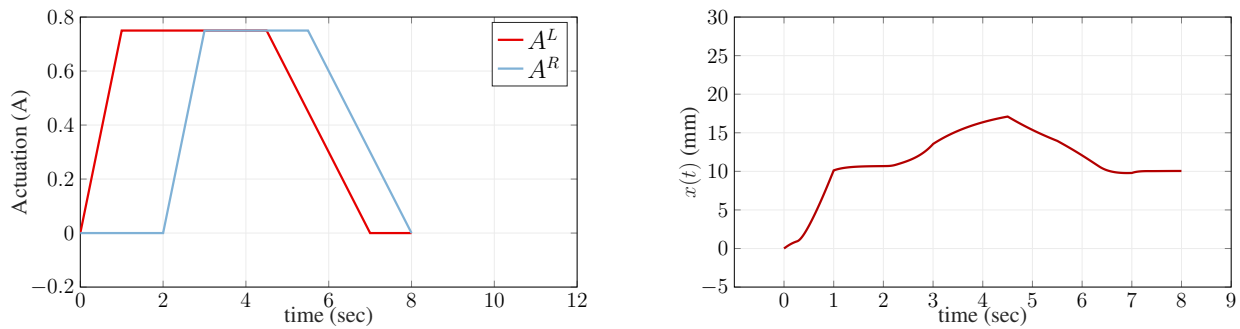


Fig. 9: **Left:** An idealized actuation gait cycle  $A$  based on the experimental gait signal traces is applied to the simulated inchworm. **Right:** The displacement of the left foot frame vs time. The displacement is 12.0% body lengths per gait. The simulated movement is qualitatively similar to the experimentally observed movement.

*Results:* For the actuation time, rise time, phase shift and time period of 4 sec, 2 sec, 2 sec and 12 sec, respectively, Fig. 8 illustrates the resulting estimates of  $A^L, A^R$ , which follow the desired symmetric trapezoidal actuation pattern. The actuation and deactivation of the estimated actuation profiles correlate to the input current signals  $I^L, I^R$ . The non-linearity of the actuation estimates can be attributed to the non-linearity related to heating and cooling of SMAs. The SMA inchworm experiences a mean displacement of 11.74 mm (13.2% of the body length) per gait cycle with a standard deviation of 1.18 mm, shown in Fig. 8. The locomotion pattern where the left foot moves in the positive direction for the duration of the actuation time (4 seconds) followed by slight movement in the negative direction thereafter is consistent with the subsequently obtained simulation results, illustrated in Fig. 9.

### B. Simulated Inchworm

A simulation of the inchworm under viscous friction with differential coefficients  $\mu_{high} = 40$  and  $\mu_{low} = 10$  was performed for a symmetric trapezoidal gait profile with a maximum actuation value of  $\bar{a} = 0.75$ . The simulated gait was designed to follow a piece-wise linear and constant version of the estimated shape actuation signals  $A$ . It varies somewhat from the true estimated gait, which has some

nonlinear response in the last part of the gait. Fig. 9(a) depicts both the periodic actuation signals  $A(t)$  and Fig. 9(b) shows the resulting movement of the body frame at the left foot. Over a single gait, the displacement was 10 mm, which is 12.0% of a body length. The experimental and simulated left foot traces are qualitatively similar and have nearly the same displacement per gait. While the derived simulation equations involved several simplifications or approximations regarding the evolution of the shape space, to first order the gross response has been captured.

## VI. CONCLUSION

Though advantageous for certain robot applications, the continuum and compliant properties of soft materials come with challenges related to robot and actuator modeling. Locomotion arises from body-environment interaction forces induced by changes in the robot's shape. For soft robots with distributed mass and actuation, the body and the actuators have non-trivial coupled dynamics. Under a periodic gait, however, the time-varying response of the soft robot may be modeled in a low-dimensional shape space. Under a known periodic shape profile, the rigid body equations for the soft robot follow naturally. External body-environment interaction forces can be modeled within the rigid body dynamics.

For an inchworm soft robot, this paper proposes a beta distribution to describe the shape during the gait, where the shape parameters are calibrated and correlate to the actuation signal. This approach considers “prior knowledge” of the robot workspace (shape changing ability) and a focus on locomotion to reduce the dimensions to two shape parameters  $A \in \mathbb{R}^2$  that directly correlate to the actuator signals (SMA input current  $I \in \mathbb{R}^2$ ). The calibration process models robot-specific complexities, including material properties, actuator-body interactions, and inter-actuator coupling. The locomotion dynamics model the frictional interactions as an external wrench acting on the body. We simulate the locomotion dynamics using viscous friction and a trapezoidal actuation profile. The actuation and displacement of the robot feet qualitatively match with the experimental results; exact reproduction of physical outcomes will be limited by parameter value uncertainty, particularly that surrounding robot-environment friction coefficients and switching criteria. The experiments reinforce that the shape-centric approach provides ‘modeling adaptability’ to accommodate for design imprecisions, actuator nonlinearities and frictional interactions of physically adaptable soft robots.

In the future, this shape-space modeling approach will facilitate learning of the robot-actuator dynamics (shape parameters) and robot-environment interactions (frictional wrench). Future work aims to jointly modify the SMA current and the gait cycle so that they may more closely match, as well as to explore other friction models. Furthermore, we would like to explore variations in the gait cycle signals to identify the optimal locomotive gait from simulation to see if it matches the experimentally discovered optimal gait.

#### REFERENCES

- [1] R. J. Webster and B. A. Jones, “Design and kinematic modeling of constant curvature continuum robots: A review,” *IJRR*, vol. 29, no. 13, pp. 1661–1683, 2010.
- [2] B. A. Jones and I. D. Walker, “Kinematics for multisection continuum robots,” *IEEE Trans. on Robotics*, vol. 22, no. 1, pp. 43–55, 2006.
- [3] F. Renda, M. Cianchetti, M. Giorelli, A. Arienti, and C. Laschi, “A 3D steady-state model of a tendon-driven continuum soft manipulator inspired by the octopus arm,” *Bioinspiration & Biomimetics*, vol. 7, no. 2, p. 025006, 2012.
- [4] F. Renda, F. Boyer, J. Dias, and L. Seneviratne, “Discrete Cosserat approach for multisection soft manipulator dynamics,” *IEEE Trans. on Robotics*, vol. 34, no. 6, pp. 1518–1533, 2018.
- [5] T. Bretl and Z. McCarthy, “Quasi-static manipulation of a Kirchhoff elastic rod based on a geometric analysis of equilibrium configurations,” *IJRR*, vol. 33, no. 1, pp. 48–68, 1 2014.
- [6] C. Duriez, “Control of elastic soft robots based on real-time finite element method,” in *IEEE ICRA*, 2013, pp. 3982–3987.
- [7] F. Faure, C. Duriez, H. Delingette, J. Allard, B. Gilles, S. Marchesseau, H. Talbot, H. Courtecuisse, G. Bousquet, I. Peterlik *et al.*, “SOFA: A multi-model framework for interactive physical simulation,” in *Soft tissue biomechanical modeling for computer assisted surgery*, 2012, pp. 283–321.
- [8] J. Hiller and H. Lipson, “Automatic design and manufacture of soft robots,” *IEEE Trans. on Robotics*, vol. 28, no. 2, pp. 457–466, 2012.
- [9] —, “Dynamic simulation of soft multimaterial 3D-printed objects,” *Soft Robotics*, vol. 1, no. 1, pp. 88–101, 2014.
- [10] S. H. Sadati, S. E. Naghibi, I. D. Walker, K. Althoefer, and T. Nanayakkara, “Control space reduction and real-time accurate modeling of continuum manipulators using Ritz and Ritz–Galerkin methods,” *IEEE Robotics and Automation Letters*, vol. 3, no. 1, pp. 328–335, 2017.
- [11] F. Boyer, V. Lebastard, F. Candelier, and F. Renda, “Dynamics of continuum and soft robots: A strain parameterization based approach,” *IEEE Transactions on Robotics*, vol. 37, no. 3, pp. 847–863, 2020.
- [12] J. Rieffel, F. Saunders, S. Nadimpalli, H. Zhou, S. Hassoun, J. Rife, and B. Trimmer, “Evolving soft robotic locomotion in PhysX,” in *11th Annual Conference Companion on GECCO: Late Breaking Papers*, ser. GECCO ’09, 2009, p. 2499–2504.
- [13] F. Saunders, E. Golden, R. D. White, and J. Rife, “Experimental verification of soft-robot gaits evolved using a lumped dynamic model,” *Robotica*, vol. 29, no. 6, pp. 823–830, 2011.
- [14] F. Saunders, B. A. Trimmer, and J. Rife, “Modeling locomotion of a soft-bodied arthropod using inverse dynamics,” *Bioinspiration & Biomimetics*, vol. 6, no. 1, p. 016001, 2011.
- [15] B. Gamus, L. Salem, A. D. Gat, and Y. Or, “Understanding inchworm crawling for soft-robotics,” *IEEE Robotics and Automation Letters*, vol. 5, no. 2, pp. 1397–1404, 2020.
- [16] B. Gamus, A. D. Gat, and Y. Or, “Dynamic inchworm crawling: Performance analysis and optimization of a three-link robot,” *IEEE Robotics and Automation Letters*, vol. 6, no. 1, pp. 111–118, 2021.
- [17] V. Vikas, P. Grover, and B. Trimmer, “Model-free control framework for multi-limb soft robots,” in *IEEE/RSJ IROS*, 2015, pp. 1111–1116.
- [18] M. M. Tanouye and V. Vikas, “Optimal learning and surface identification for terrestrial soft robots,” in *IEEE RoboSoft*, 2018, pp. 443–448.
- [19] D. M. Rincon and J. Sotelo, “Ver-vite: dynamic and experimental analysis for inchwormlike biomimetic robots,” *IEEE Robotics & Automation Magazine*, vol. 10, no. 4, pp. 53–57, 2003.
- [20] W. Tang, F. Reyes, and S. Ma, “Study on rectilinear locomotion based on a snake robot with passive anchor,” in *IEEE/RSJ IROS*, 2015, pp. 50 – 955.
- [21] W. Saab, P. Racioppo, A. Kumar, and P. Ben-Tzvi, “Design of a miniature modular inchworm robot with an anisotropic friction skin,” *Robotica*, vol. 37, no. 3, pp. 521–538, 2019.
- [22] D. Li, K. Wang, W. Wang, H. Zhang, and G. Zong, “Analysis of gait control of wall-climbing caterpillar robot,” in *IEEE ROBIO*, 2009, pp. 1929–1934.
- [23] A. Chang and P. Vela, “Evaluation of bio-inspired scales on locomotion performance of snake-like robots,” *Robotica*, vol. 37, no. 8, 2019.
- [24] G. S. Chirikjian and J. W. Burdick, “Kinematics of hyper-redundant robot locomotion with applications to grasping,” in *IEEE ICRA*, 1991, pp. 720–725 vol.1.
- [25] G. Chirikjian and J. Burdick, “The kinematics of hyper-redundant robot locomotion,” *IEEE Trans. on Robotics and Automation*, vol. 11, no. 6, pp. 781–793, 1995.
- [26] A. Chang and P. Vela, “Shape-centric modeling for control of traveling wave rectilinear locomotion on snake-like robots,” *Robotics and Autonomous Systems*, vol. 124, p. 103406, 2020.
- [27] F. Boyer, S. Ali, and M. Porez, “Macrocontinuous dynamics for hyper-redundant robots: Application to kinematic locomotion bioinspired by elongated body animals,” *IEEE Trans. on Robotics*, vol. 28, no. 2, pp. 303–317, 2012.
- [28] F. Boyer and M. Porez, “Multibody system dynamics for bio-inspired locomotion: from geometric structures to computational aspects,” *Bioinspiration & Biomimetics*, vol. 10, no. 2, p. 025007, 2015.
- [29] A. Chang, M. Serrano, and P. Vela, “Shape-centric modeling of lateral undulation and sideward gaits for snake robots,” in *IEEE CDC*, 2016, pp. 6676 – 6682.
- [30] T. Umedachi, V. Vikas, and B. Trimmer, “Softworms: the design and control of non-pneumatic, 3D-printed, deformable robots,” *Bioinspiration & Biomimetics*, vol. 11, no. 2, p. 025001, 2016.
- [31] T. Umedachi, V. Vikas, and B. A. Trimmer, “Highly deformable 3-D printed soft robot generating inching and crawling locomotions with variable friction legs,” in *IEEE/RSJ IROS*, 2013, pp. 4590–4595.
- [32] V. Radhakrishnan, “Locomotion: dealing with friction,” *PNAS*, vol. 95, no. 10, pp. 5448–5455, 1998.
- [33] J. Ostrowski, “The mechanics and control of undulatory robotic locomotion,” Ph.D. dissertation, California Institute of Technology, 1996.